Self-testing randomness from a nuclear spin system

Xing Chen,[1] Minsik Kwon,[1] Vadim Vorobyov,[1] Jörg Wrachtrup,[1,2] and Ilja Gerhardt[3]

[1]*3. Institute of Physics, University of Stuttgart and Institute for Quantum Science and Technology (IQ^{ST}), Pfaffenwaldring 57, D-70569 Stuttgart, Germany*
[2]*Max Planck Institute for Solid State Research, Heisenbergstraße 1, D-70569 Stuttgart, Germany*
[3]*Institute for Solid State Physics, Appelstraße 2, D-30167 Hannover, Germany*

Randomness is a very important resource for cryptography, algorithms, and scientific simulations. Since all classical processes are considered to be intrinsically deterministic, we must build quantum random number generators which utilize quantum processes to generate true randomness. Quantum random number generators have been realized in different quantum systems, including quantum optical systems, and trapped ions. Here we present a proof-of-concept random number generator based on a nuclear spin system for the first time. The state preparation and measurements are performed with high-fidelity operations in our system. The entropy of randomness in the experimental data is quantified by two dimension witness certification protocols, which require no detailed models to describe the experimental devices but only some general assumptions, such as the limited dimensionality and the independence of the experimental devices.

I. INTRODUCTION

Randomness is a very valuable resource and has many applications in scientific research, cryptography, and entertainment, such as lottery and gambling. Since the collapse of a quantum superposition state is intrinsically random [1], the generation of true random numbers relies on this unpredictable collapse of quantum superposition states [2–6]. However, in any real-world experiments, such true randomness from quantum superposition is always crippled by undesired noise or misalignment of the experimental devices. Therefore, it is important to certify true randomness from the imperfect experimental results.

This goal can be achieved with quantum randomness certification protocols based fundamental physics inequalities, such as Bell inequalities [2, 6–9], Koch-Specker inequality [10, 11], and dimension witness [12, 13]. Such protocols have been implemented in different platforms, including trapped ions [2, 11], and photonic setups [6, 8, 12].

The nuclear spin system inside the NV color center is well isolated from the environment and can be operated at room temperature. Their creation and control are relatively easy [14–16]. This stable quantum system has been used in the quantum computing area for years [16–18]. As far as we know, the nuclear spin system has not been used to generate quantum randomness, here we present a quantum random generator based on it. We use dimension witness [19] as the physics inequality to construct our randomness certification protocols.

The protocols we present here are semi-device-independent (SDI) protocols. *SDI* means that the raw measurement outcomes reveal their quantumness if a certain number of assumptions of the experimental setup can be guaranteed. For the semi-device-independent protocols mentioned in this article, the assumptions about the experimental devices should be general, which means they are not supposed to characterize the devices in detail, and they do not belong to source-independent or measurement-device-independent protocols. Among these we find the Kochen-Specker inequality [10, 11] and the dimension witness [12, 19, 20]. Our protocols here are inspired by [12, 19]. In [12], the authors utilized a 2-dimensional dimension witness W_2 to quantify the entropy in the randomness. In our work here, we extend this model into a three-dimensional Hilbert space and develop two different methods to quantify the entropy of the randomness from the prepare-and-measure (P&M) scenario based on the nuclear spin states.

This paper is organized as follows. In section II, we describe the P&M scenario of the protocol, and then we explain how we realize it in a nuclear spin state inside a single NV color center. In section III, we illustrate our two protocols in detail. Then in section IV, we analyze the data and show the experimental results.

II. PREPARE-AND-MEASURE SCENARIO

In each run of the P&M scenario, Alice prepares one state ρ_a, which can be represented as

$$\rho_a = \frac{1}{2}(\mathbf{I} + \vec{S}_a \cdot \vec{\sigma}),$$

where $\vec{S}_a$ ($a = \{0, 1, 2, 3, 4, 5\}$) denotes Bloch vectors of the prepared state, and $\vec{\sigma} = (\sigma_x, \sigma_y, \sigma_z)$ is the Pauli vector. Afterwards, Bob measures the states in measurement basis M_b

$$M_b = \vec{T}_b \cdot \vec{\sigma},$$

where $\vec{T}_b$ ($b = \{0, 1, 2\}$) is the Bloch vector of the measurement settings. After the measurement, Bob gets a binary result $m = \{0, 1\}$. $\{m, a, b\}$ forms a raw event [21].

In our experiment, the normal P&M scenario is slightly altered: Alice and Bob are in the same location, it means

after Alice prepares the state, Bob does the measurement in the location where the state is prepared.

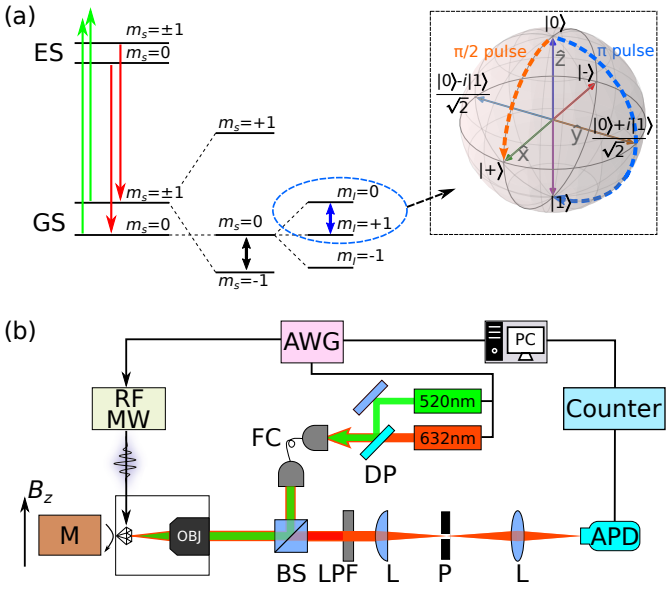

FIG. 1: **(a)** Energy level of NV^- state, where **ES** means excited state and **GS** means ground state. We choose the nuclear spin states $|0_I\rangle$ and $|+1_I\rangle$ to prepare our states, which is shown in a bloch-sphere on the right. **(b)** The sketch of the experimental setup. In the figure, **M** represents the permanent magnet, **RF** means radio-frequency pulse, **MW** means microwave pulse, **OBJ** means objective, **FC** means fiber coupler, **AWG** means arbitrary waveform generator, **DP** means dichroic polarizer, **BS** means beam-splitter, **LPF** means long pass filter, **L** means lens, **P** means pinhole, **APD** means avalanche photodiode, and **Counter** here is a timetagger. We use a 532 nm laser to pump the NV into NV^-, and a 632 nm laser to to intensify the zero photon line.

II.I. Experimental setup

Nuclear spin states of NV centers in a diamond are very stable quantum systems [15, 16, 22–24], and with the so-called single-shot readout technique [24], the nuclear spin state can be probed with very high fidelity. The nuclear spin states used in our protocol are from the nucleus of a nitrogen atom [^{14}N] of a negatively charged NV center. The energy level of the NV^- and a sketch of our experimental setup is shown in Fig. 1.

First, we use a pulse of a 520 nm green laser to initialize the NV center into the negatively charged state NV^-, and the electron spin state into $|0_e\rangle$ (corresponds to $m_S = 0$). In the mean time, the nuclear spin state is in an incoherent mixture of the its eigenstates $|-1_I\rangle$, $|0_I\rangle$, and $|+1_I\rangle$ ($m_I = -1, 0, +1$). Then we apply a series of microwave (MW) π pulses and radio-frequency (RF) π pulses to initialize the nuclear spin states from $|0_I\rangle$, $|+1_I\rangle$ into $|-1_I\rangle$. The charge state preparation and nuclear spin state initialization fidelities are decided by the thresholds, which is discussed later.

After the initialization stage, we can start our P&M protocol. As shown in Fig. 2 (a), in the state preparation step we apply a RF π pulse between $|-1_I\rangle$ and $|0_I\rangle$ ($R_y^{-1,0}(\pi)$) to flip the spin state from $|-1_I\rangle$ into $|0_I\rangle$, which corresponds to state $|0\rangle$. Depending on the state we intend to prepare, another RF pulse $R_i^{0,+1}(\theta)$ along the axis i ($i \in \{x, y, z\}$) can be applied. For instance, by applying a RF pulse $\pi/2$ along the y axis ($R_y^{0,+1}(\pi/2)$), nuclear spin will be in state $(|0_I\rangle + |1_I\rangle)/\sqrt{2}$, which corresponds to state $|+\rangle$.

Following the state preparation, we measure the prepared nuclear spin state. Take state $|+\rangle$ as an example, we measure it in basis $\hat{z}$. The state $|+\rangle$ is a superposition state of $|0_I\rangle$ and $|+1_I\rangle$. Because of the hyperfine interaction of the electron spin and the intrinsic ^{14}N nuclear spin of the NV defect, the transition frequency of the electron spin is dependent on the state of the nuclear spin. So, we can apply a MW π pulse to flip the electron spin state conditioned on the nuclear spin state (e.g., $|0_I\rangle|0_e\rangle \rightarrow |0_I\rangle|0_e\rangle$, $|+1_I\rangle|0_e\rangle \rightarrow |+1_I\rangle|-1_e\rangle$). This is exactly a controlled-not operation [24]. Since the nuclear spin is in state $|+\rangle$, by this controlled-not operation, the electron spin will be in a superposition state of $|0_e\rangle$ and $|-1_e\rangle$. Because the fluorescence intensity differs by roughly a factor of 2 for electron spin states $|0_e\rangle$ and $|-1_e\rangle$ [24, 25], these target states can be distinguished by shining in a short laser pulse.

With a short laser pulse, the electron spin state collapses into either $|0_e\rangle$ or $|-1_e\rangle$ with equal probability, correspondingly the nuclear spin state collapses into $|0_I\rangle$ and $|+1_I\rangle$ with equal probability. However, because of the low collection efficiency, the difference in fluorescence intensity is not distinguishable with one repetition. Therefore, we repeat this quantum non-demolition (QND) protocol [24] 1000 times to realize the single-shot readout of the nuclear spin state. The results give us a fluorescence intensity distribution where each peak corresponds to different nuclear spin states. This fluorescence intensity distribution is a photon-counting histogram, which should have two peaks with the same area if the nuclear spin state collapses into $|0_I\rangle$ and $|-1_I\rangle$ with equal probability. However, as shown in the right part of Fig. 2 (a), the distribution is not balanced. A major reason is the imperfect state initialization, including the charge state initialization of the NV center and the nuclear spin state initialization. This could be confirmed with a single-shot readout after each step of the initialization. After we use a 520 nm laser to prepare the negatively charged state NV^-, we perform a single-shot readout of the charged state. The distribution of the fluorescence intensity in each charged state readout is shown in the left part of Fig. 2 (b). The peak with larger fluorescence intensity corresponds to NV^-, and the one with lower fluorescence

intensity corresponds to NV^0. From this figure, we find that not all the NV centers are being pumped into the NV^- state. Next, we apply a series of MW and RF π pulse to initialize the nuclear spin states into $|-1_I\rangle$. After this step, we do another single-shot readout of the nuclear spin states. The photon-counting histogram is shown as the middle figure of Fig. 2 (b). As expected, we cannot initialize all nuclear spin states into $|-1_I\rangle$.

As shown in Fig. 2 (b), the histograms of the charged states and initialized nuclear spin states both have two overlapped peaks. Each peak represents a different state, the neutrally charged state NV_0, the undesired spin state $|0_I\rangle$ and $|+1_I\rangle$ after initialization contributes extra fluorescence intensity distribution to the preliminary results and make it unbalanced. To make the distribution of preliminary results balanced, we need to discard the undesired states in charged stated decision and nuclear spin initialization stages. First, we need to set thresholds for the two histograms, so that the states in the two peaks can be distinguished precisely. With the thresholds being settled, the fidelities of charged state decision and nuclear spin state initialization is $F_1 = 1 - \epsilon_1$ and $F_2 = 1-\epsilon_2$, where $\epsilon_{1,2}$ are the corresponding errors when distinguishing the states in the two histograms with the given thresholds.

The thresholds in Fig. 2 (b) are decided by 10% sample data before the generation of randomness (see supplementary for details). After setting thresholds in the left two single-shot readout histograms of Fig. 2 (b), and discarding the undesired states, the distribution of the final nuclear spin states, which is shown on the right figure of Fig. 2 (b), are balanced. We assign the left peak as random bit "1", and the right peak as "0". Clearly, the distribution of raw bits are not perfectly separated from each other, a small fraction of them are still overlapped. In order to distinguish the results unambiguously, we also need to set a threshold for the raw bits histogram.

In Fig. 3 (a), the threshold is fixed for the measurement results of all 18 different P&M pairs (six preparations and three measurements, in total, there are 18 different P&M pairs) in the first data-set [26]. With the threshold being settled, the probability distribution of getting a raw bit 0 for each P&M combination and their corresponding error bars are shown Fig. 3 (b).

After fixing the thresholds for charged state decision, nuclear spin state initialization, and the raw bits, the total fidelity of each P&M pair can be calculated by the following equation

$$F_{\text{total}} = F_1 \cdot F_2 \cdot F_3 \tag{1}$$

where $F_3 = 1 - \frac{\epsilon_l+\epsilon_r}{2}$, and $\epsilon_{l,r}$ are the errors in each histogram when applying the green dashed line as threshold to distinguish bits "1" and "0" in Fig. 3 (a).

Because of the limited memory size of the setup, we can only input one sequence with 36 different P&M pairs each time. In this one sequence, if we input pairs randomly, it is infeasible to implement all 18 possible pairs. This makes it very difficult to investigate the memory effect of each pair. To show that our setup is memoryless for any P&M pair, we specially design a sequence with 324 pairs. During our experiment, we divide these 324 pairs into 9 different sections, and each section contains 36 pairs. All the 324 pairs can be implemented in every 9 input sequences. The 324 pairs are designed in such a way that each of the 18 P&M pairs appears with the same frequency, and after the current pair, all the 18 different pairs appear with the same frequency in the next coming pair. For example, for the P&M pair S_0-$\hat{z}$, the next P&M pair can be any pair from all the 18 pairs. In this way, we can analyze the memory effect of S_0-$\hat{z}$ on all the pairs instead of just a fraction of them.

In order to quantify the memory effect of our experimental setup, we calculate the differences of conditional probabilities of the adjacent P&M runs. There are four conditional probabilities $p(1|0)$, $p(1|1)$, $p(0|0)$, $p(0|1)$. Among them, $p(1|0)$ means, the probability of getting results "1" in the current P&M run, with result "0" from previous run. The other three conditional probabilities have similar definitions. Ideally, all these conditional probabilities should be 0.5, which means the previous measurement result does not affect the next coming measurement result. In other words, $p(1|0) - p(1|1) = p(0|1) - p(0|0) = 0$. So we can use the difference between $p(1|0)$ and $p(1|1)$ or $p(0|1)$ and $p(0|0)$ to indicate the memory effect of our experimental setup. Since $p(1|0) - p(1|1) = p(0|1) - p(0|0)$ always holds true, we only use the difference $p(1|0) - p(1|1)$ in the following calculation.

We investigate the memory effect of each individual P&M pair. Considering the i-th and the $(i+1)$-th P&M run, there will be a joint event $\{m_i, a_i, b_i, m_{i+1}, a_{i+1}, b_{i+1}\}$. We want to show that for any $\{a_i, b_i\}$, the result m_i does not affect the distribution of m_{i+1}. This can be represented as the differences between the conditional probabilities $p(1_{i+1}|0_i)$ and $p(1_{i+1}|1_i)$. In Fig. 3 (c), such differences of each P&M pair are shown. Take the first bar as an example, the i-th P&M pair here is S_0-$\hat{z}$. As expected, all the conditional probability differences can be explained by the 3σ shot noise, so our nuclear spin state quantum randomness generation system is memoryless.

With the raw bits from our memoryless experimental setup, next, we develop two dimension witness [19] protocols to quantify the randomness in the raw bits.

III. MODEL ILLUSTRATION

Before we proceed with the dimension witness protocols, we describe the assumptions needed for our two protocols. The assumptions here mentioned are similar to the assumptions in [12, 27], but for the self-consistence of

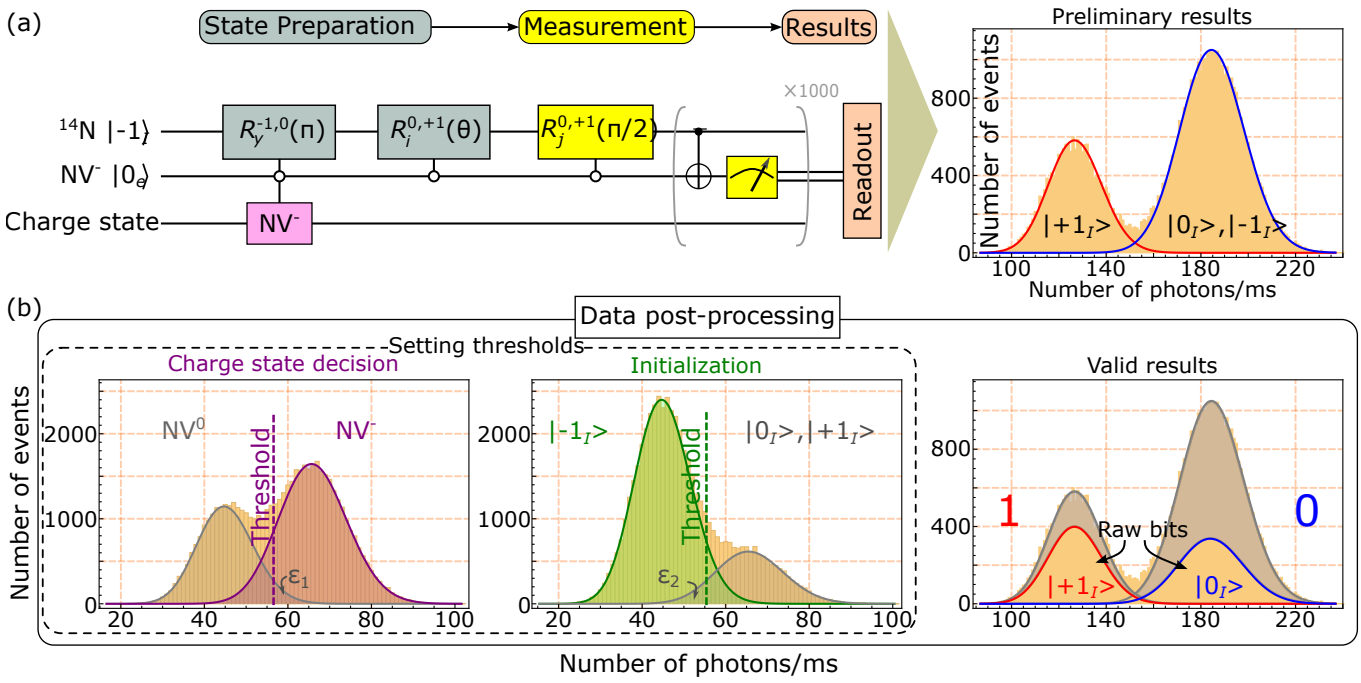

FIG. 2: The P&M scenario and the data post-processing, all the histograms are fitted by Gaussian distributions (solid lines). **(a)** Quantum circuit representation of our P&M scenario. First, we pump the NV color center into NV$^-$ and initialize the nuclear spin state of ^{14}N into $|-1_{\rm I}\rangle$. Then in the state preparation step, we apply a π pulse to this nuclear spin state and rotate it into $|m_I=0\rangle$, which corresponds the state $|0\rangle$. With further π or $\pi/2$ pulses, the other five states $|1\rangle, |+\rangle, |-\rangle, \frac{|0\rangle+i|1\rangle}{\sqrt{2}}$, and $\frac{|0\rangle+i|1\rangle}{\sqrt{2}}$ can be prepared. This is represented as $R_i^{0,+1}(\theta)$ $(\theta=\{\pi,\pi/2\})$ in the figure. In the measurement step, we apply a $\pi/2$ pulse $(R_j^{0,+1}(\pi/2))$ along the $\hat{x},\hat{y}$ or $\hat{z}$ axis to perform a corresponding measurement, then single-shot readout is used to get the state of the nuclear spin system. **(b)** In the post-processing process, we set thresholds for the charged state and nuclear spin state initialization distribution histograms. Then we get balanced raw bits from the unbalanced preliminary results. In the initialization histogram, the green part (left) is the spin state $|-1_{\rm I}\rangle$ we desire, and the grey part needs to be filtered out. Since there is overlapping area between these two distributions, we need to set a threshold. For the charge state single-shot readout histogram, the NV$^-$ is the right peak, which is what we intend to utilize. ϵ_1 and ϵ_2 are the corresponding errors of choosing the given thresholds in the histograms. In the valid results (raw bits) histogram, we assign left peak as raw bits "1", and right peak as "0".

this work, we rephrase them here. Our two protocols are based on the same experimental device, they require the same assumptions: (1) the state preparation and measurement settings (a,b) are not determined beforehand and are unpredictably chosen; (2) the preparation and measurement devices are independent from each other; (3) the information in the measurement results of each side is contained in a two-dimensional quantum subspace; (4) the system is memoryless and subsequent outcomes are not directly correlated.

Our P&M protocol is done in the same location, it is important that the state preparation and measurement devices are independent from each other, and this requirement is fulfilled by assumptions (1) and (2). Assumption (1) also implies that the devices that are used to generate the input strings a,b are not correlated with the measurement devices. Subsequently, a,b can be pseudo-random numbers, as long as they are independent from each other and the measurement apparatus. Assumption (2) can be easily realized if the experimental devices are not manufactured by malicious producers. In our case, the state preparation device and the measurement device are error-prone, but we assume their errors are independent from each other, and there are no pre-established correlations between the two devices. Assumption (3) means that the measurement results of each measurement setting can be described by a qubit. About assumption (4), it requires the previous measurement result of the device does not affect the measurement result of the following measurement. From Fig. 3 (c) we can see that this assumption can be fulfilled by our experimental setup.

III.I. First Model description

In the model of [12], the P&M scenario is done in a two-dimensional Hilbert space (i.e. a plane). In our

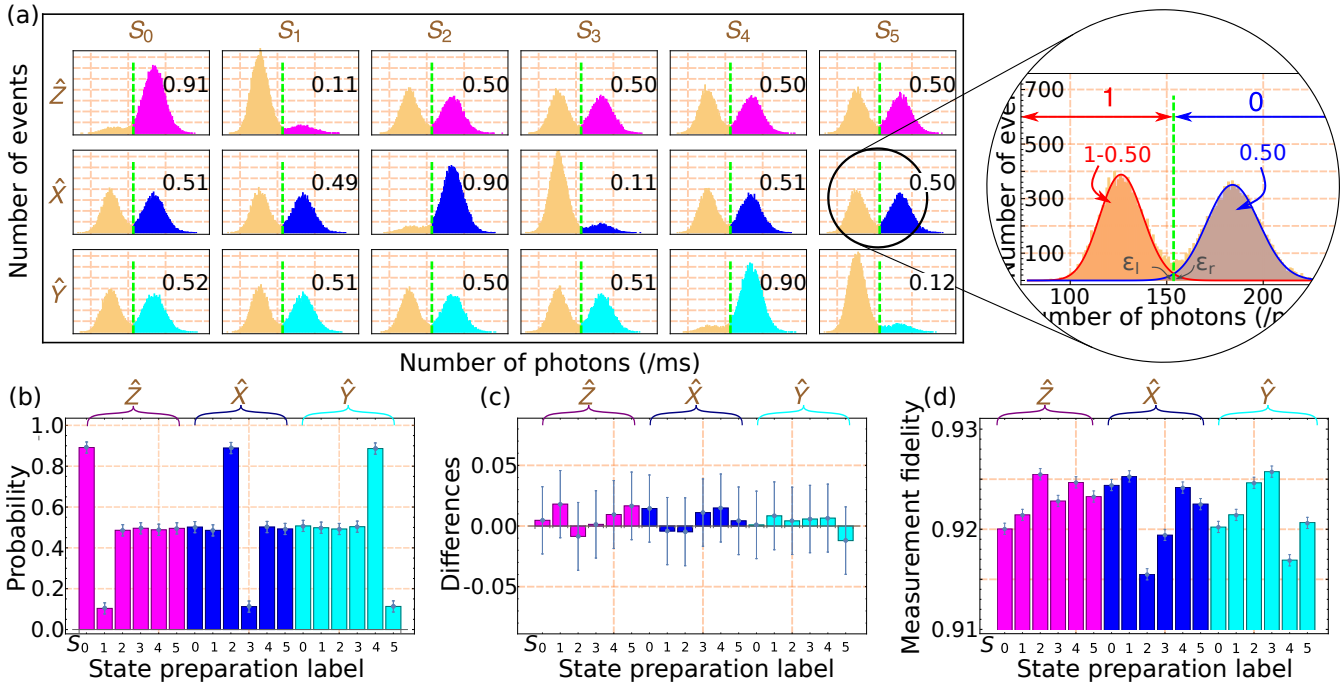

FIG. 3: Experimental results analysis for raw results in the first data-set. **(a)** Photon-counting distribution of 18 different P&M pairs. The vertical axis of all 18 sub-figures is the number of events for different photon counts, and the horizontal axis is the number of photon counts. The dashed green line is the threshold line that is used to differentiate the raw bits "1" and "0". The photon counts value of the green dashed line here is 153, and in the supplementary, we show how to get this threshold in detail. In the right big circle of this sub-figure, the photon counts distribution of one specific P&M ($S_5 - \hat{x}$) is shown. The probability of getting "1" is calculated by the photon counts which are smaller than the threshold line, and "0" is the photon counts which are larger than the threshold line. $\epsilon_{l,r}$ are the measurement errors of each peak when applying the green dashed line as a threshold. **(b)** The probability distribution in this chart is the probability of getting the result "0" in the measurement of sub-figure (a). At the top of each bar, the 3σ shot noise is shown. **(c)** Conditional probability differences of different P&M pairs. In this figure, we can see that the conditional probability differences are not zero, but they can all be explained by the 3σ shot noise. In other words, our experimental setup can be considered as memoryless. **(d)** Total fidelity of each P&M pair.

work, we extend this original model into a three dimensional Hilbert space, more specifically, three mutually orthogonal planes. The state ρ_a, which is prepared by Alice, is randomly chosen from six possible preparations : $\vec{S}_0 = -\vec{S}_1 = \hat{z}$, $\vec{S}_2 = -\vec{S}_3 = \hat{x}$ and $\vec{S}_4 = -\vec{S}_5 = \hat{y}$. After the preparation, Bob measures the states in measurement bases : $\vec{T}_0 = \hat{z}$, $\vec{T}_1 = \hat{x}$ and $\vec{T}_2 = \hat{y}$, and gets binary results m. $\{m, a, b\}$ forms a raw event for each run of the experiment.

In the experimental scheme above, the state preparations and measurements can be categorized into three planes, and in each plane a two dimensional dimension witness W_2 can be constructed. For instance, in the Bloch sphere of Fig. 1(a), within $xz-$plane, the states $|0\rangle, |1\rangle, |+\rangle, |-\rangle$, measurement bases $\hat{x}, \hat{z}$, and the measurement results can be used to construct a 2-dimensional dimension witness $W_{\rm xz}$. The dimension witness $W_{\rm xy}$ in the $xy-$plane and the dimension witness $W_{\rm yz}$ in the $yz-$plane can be constructed in a similar fashion.

Since three different 2-dimensional dimension witnesses can be constructed in different planes, we use the equation in [12] three times. In each use of the protocol we only utilize $\frac{4}{9}$ raw bits data [28], so the total output entropy is $3 \times \frac{4}{9} \times 0.23 = 0.31$ bits per event in an ideal case. While for the original 2-dimensional dimension witness only 0.23 bits per event randomness can be certified per event in an ideal case.

In each plane we utilize 4/9 data to construct a W_2, we have three different planes, and $4/9 \times 3 \geq 1$, this dose not mean the model is inconsistent with the data. Since in our protocol, some of the measurement results are reused to construct W_2 in different planes. Take plane xz and yz as examples. In the xz plane, we use states $|0\rangle, |1\rangle, |+\rangle, |-\rangle$ and measurement bases $\hat{x}, \hat{z}$ to construct the dimension witness $W_{\rm xz}$, while in the yz plane, state $|0\rangle, |1\rangle, \frac{|0\rangle+i|1\rangle}{\sqrt{2}}, \frac{|0\rangle+i|1\rangle}{\sqrt{2}}$ and measurement bases $\hat{y}, \hat{z}$ are used to construct the dimension witness $W_{\rm yz}$. The states $|0\rangle, |1\rangle$ and measurement basis $\hat{z}$ are reused, but the final quantified entropy in the randomness is not repeated in two different planes, because the randomness generation (in the xz plane) is completed by quantum states $|0\rangle, |1\rangle$ in measurement $\hat{x}$, and states $|+\rangle, |-\rangle$ in measurement $\hat{z}$. These state-measurement combinations are not use again in the construction of $W_{\rm yz}$ in the yz plane,

so the quantified entropy is not repeated in the results. The reused combinations (such as $|0\rangle, |1\rangle$ with $\hat{z}$) have determined outcomes and cannot be utilized to generate randomness.

The limitation of this protocol is obvious, as mentioned, it is a repeated usage of the W_2 protocol in [12]. In our experiment scheme, the states and measurements are in the intersection lines of $xy-$, $xz-$, and $yz-$ planes. So we can reuse some state-measurement pairs to construct different W_2 dimension witnesses, and this gives us some advantages to certify more randomness per raw bit. This also means that the protocol can only be applied to the specific states and measurements which are distributed in the intersection lines of three different planes in a Bloch sphere. If the six preparations S_a and three measurements T_b cannot form three different planes, this protocol will be inapplicable. Take our current experimental scheme as an example, we rotate $|0\rangle$ and $|1\rangle$ with angle $0 < \theta < \pi/2$ in the $xz-$plane of the Bloch sphere. After the rotation, dimension witness W_{xz} and W_{xy} can still be constructed, but W_{yz} cannot be calculated, since $|0\rangle$ and $|1\rangle$ are not in the $yz-$plane, and there are only two states left in this plane. To improve the situation here, we develop our second dimension witness randomness certification protocol.

III.II. Second Model description

There is another way to certify more randomness from the same data. Our first protocol is based on the W_2 protocol [12], and in an ideal case, the entropy in the output randomness is 0.31 bits per raw bit. In our second protocol, we utilize a 3-dimensional dimension witness W_3 (defined below) to quantify the entropy of the randomness, the entropy increases to 0.34 bits per raw bit.

In order to construct W_3, we need 6 preparation states and 3 measurement bases [19]. The states in preparation need to be in a dimension d which is larger than $\sqrt{3}$, so we can get a nonzero W_3 and then we can quantify the quantumness involved in the measurement process by W_3.

There are six input states ρ_a in our experiment, and correspondingly three measurement bases. The Hilbert space of each state has a dimension $d = 2$, which is larger than $\sqrt{3}$, so a three dimensional dimension witness W_3 can be constructed for our experimental scheme. This W_3 is defined as

$$W_3 = \begin{vmatrix} p(0,0)-p(1,0) & p(2,0)-p(3,0) & p(4,0)-p(5,0) \\ p(0,1)-p(1,1) & p(2,1)-p(3,1) & p(4,1)-p(5,1) \\ p(0,2)-p(1,2) & p(2,2)-p(3,2) & p(4,2)-p(5,2) \end{vmatrix} \tag{2}$$

where $p(a,b)$ means measuring state a in measurement basis b, the probability of getting a result m (chosen as 0 here). When $0 < W_3 \leq 1$, quantumness is involved in the measurement. This quantumness means the measurement results is not deterministic and thus we can certify randomness from the measurement results.

The entropy of the randomness per raw bit is quantified by the conditional min-entropy $H_\infty(M|AB)$ (where M, A, B represent the sets of random variables m, a, b). It is defined as $H_\infty(M|AB) = -\log_2 p_{\mathrm{guess}}$. Assuming uniformly distributed input a and b, the guessing probability p_{guess} is derived as [29]

$$\begin{aligned} p_{\mathrm{guess}} &= \frac{1}{18}\sum_{a,b}\max_m p(m|a,b) \\ &\leq \frac{1}{3}\max_a \sum_b \max_m p(m|a,b) \\ &\leq \frac{1}{2}\left(1+\sqrt{1-\frac{2}{3}\left(1-\sqrt{1-\frac{1}{4}\left(1-2\sqrt[6]{\left(8{W_3}^2+1\right)^3}\cos\left(\frac{1}{3}\left(\tan^{-1}\left(\frac{8W_3\sqrt{\left(1-W_3^2\right)^3}}{-8{W_3}^4-20{W_3}^2+1}\right)+\pi\right)\right)\right)}\right)}\right) \end{aligned} \tag{3}$$

Suppose the preparation states and measurement bases are the same as previous model: $\vec{S}_0 = -\vec{S}_1 = \vec{T}_0 = \hat{z}$, $\vec{S}_2 = -\vec{S}_3 = \vec{T}_1 = \hat{x}$ and $\vec{S}_4 = -\vec{S}_5 = \vec{T}_2 = \hat{y}$. Then in each round of the protocol, we choose settings among the six possible preparations $a = \{0,1,2,3,4,5\}$, and three measurement bases $b = \{0,1,2\}$, resulting in a binary outcome $m = \{0,1\}$. If distribution of preparations a and measurements b are uniform, then $W_3 = 1$ can be reached. In this case, the min-entropy is $H_\infty(M|AB) = -\log_2 p_{\mathrm{guess}} = 0.34$ bits per raw bit. When the system is in a non-ideal situation, e.g., misaligned, we will get $0 < W_3 < 1$, but still the guessing

Data	W_3	R_{w_3}[bits]	W_{xz}	W_{yz}	W_{xy}	R_{w_2}[bits]	F_{total}
#1	0.50	35632	0.63	0.64	0.62	23525	$92 \pm 0.31\%$
#2	0.46	34770	0.60	0.60	0.59	22364	$90 \pm 0.30\%$
#3	0.51	33057	0.64	0.64	0.63	21946	$92 \pm 0.31\%$
SUM		103459				67835	

TABLE I: The analysis results for three different data-sets. The first column is the label of each data-set. R_{w_3} means the random bits extracted by the W_3 model, R_{w_2} means the random bits extracted by the W_2 model. The last row shows the sum of the extracted random bits in all the three data-sets with two different protocols.

probability in Eqn. 3 is larger than 0.5, and quantum randomness can be certified.

IV. RESULTS ANALYSIS

The experimental running time in total is about 21 hours. It is split into three different days, the running time in each day is about 7 hours, so we got three different data sets. Each data-set contains 418666, 453829, and 381796 raw events, in total, we have 1.25×10^6 raw events. In the W_2 model, with a confidence level of 99%, and hashing error 0.001 [30], the total extractable random bits from all data-sets are 67835 bits, and the randomness generation speed is about 0.87 bits per second. While in our W_3 model, with the same confidence level and hashing error, the total extractable random bits are 103459 bits from all data-sets, the randomness generation speed is about 1.33 bits per second. The value of dimension witness and extracted random bits of each data-set is shown in Table. I. For the details of randomness extraction, please refer to the supplementary material.

In Fig. 4. The theoretical curves of our W_3 and W_2 models are shown. For W_2 model, there are three W_2 values (W_{xz}, W_{yz} and W_{xy}) for each data-set, but we only show the average value $W_2 = (W_{\text{xz}} + W_{\text{yz}} + W_{\text{xy}})/3$ for each data-set. From the above analysis, we can see that in our experimental data, compared with W_2 model, 53% more random bits can be certified by W_3 model.

V. CONCLUSION

We generate quantum randomness from a nuclear spin system in a negatively charged single NV center at room temperature and quantify the entropy in the randomness with two different models. Both models are based on the dimension witness [19], while their dimensionalities are not the same. The first model is a different application of the protocol in [12]. In our second dimension witness model, we develop a randomness certification protocol based on a three-dimensional dimension witness W_3. We have demonstrated how to certify randomness from our experimental data using the two different models.

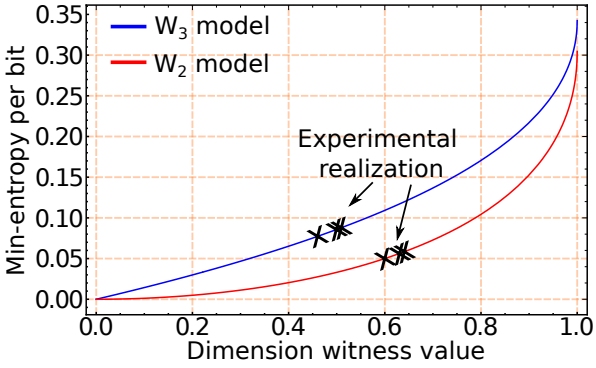

FIG. 4: Output randomness per raw bit by utilizing different dimension witnesses protocols. The blue curve (the upper curve) is the theoretical curve of the W_3 model, and the red curve (the lower curve) represents the theoretical curve of the W_2 model. The crosses in the blue and red curves are the experimental realization of our two different protocols, we have three different data sets, each cross represents each data set.

For the first model, the application is relatively limited to a special case where states preparation and measurements are distributed in the intersection lines of three planes, and in our case, these three planes are the $xz-$plane, $xy-$plane, and $yz-$plane in a Bloch sphere. The second model is based on a 3-dimensional witness W_3, and it can be applied to any P&M scenario with six input states, three measurement bases, and binary results. Also, from our experimental data, the model based on W_3 can certify 53% more random bits than the W_2 model.

Our experimental setup and data analysis shows that it is feasible to build a quantum random number generator with a nuclear spin system.

[1] L. D. Landau and E. M. Lifshitz, *Quantum mechanics: non-relativistic theory*, vol. 3 (Elsevier, 2013).

[2] S. Pironio, A. Acín, S. Massar, A. B. de la Giroday, D. N. Matsukevich, P. Maunz, S. Olmschenk, D. Hayes, L. Luo, T. A. Manning, et al., Nature **464**, 1021 EP (2010), URL https://doi.org/10.1038/nature09008.

[3] A. Acín, S. Massar, and S. Pironio, Phys. Rev. Lett. **108**, 100402 (2012), URL https://link.aps.org/doi/10.1103/PhysRevLett.108.100402.

[4] A. Acín and L. Masanes, Nature **540**, 213 (2016), ISSN 1476-4687, URL https://doi.org/10.1038/nature20119.

[5] M. Herrero-Collantes and J. C. Garcia-Escartin, Rev. Mod. Phys. **89**, 015004 (2017), URL https://link.aps.org/doi/10.1103/RevModPhys.89.015004.

[6] L. Shen, J. Lee, L. P. Thinh, J.-D. Bancal, A. Cerè, A. Lamas-Linares, A. Lita, T. Gerrits, S. W.

Nam, V. Scarani, et al., Phys. Rev. Lett. **121**, 150402 (2018), URL https://link.aps.org/doi/10.1103/PhysRevLett.121.150402.

[7] J. S. Bell, Physics Physique Fizika **1**, 195 (1964), URL https://link.aps.org/doi/10.1103/PhysicsPhysiqueFizika.1.195.

[8] P. Bierhorst, E. Knill, S. Glancy, Y. Zhang, A. Mink, S. Jordan, A. Rommal, Y.-K. Liu, B. Christensen, S. W. Nam, et al., Nature **556**, 223 (2018), ISSN 1476-4687, URL https://doi.org/10.1038/s41586-018-0019-0.

[9] Y. Liu, Q. Zhao, M.-H. Li, J.-Y. Guan, Y. Zhang, B. Bai, W. Zhang, W.-Z. Liu, C. Wu, X. Yuan, et al., Nature **562**, 548 (2018), ISSN 1476-4687, URL https://doi.org/10.1038/s41586-018-0559-3.

[10] S. Kochen and E. P. Specker, Journal of Mathematics and Mechanics **17**, 59 (1967), ISSN 00959057, 19435274, URL http://www.jstor.org/stable/24902153.

[11] M. Um, X. Zhang, J. Zhang, Y. Wang, Y. Shen, D.-L. Deng, L.-M. Duan, and K. Kim, Scientific Reports **3**, 1627 EP (2013), article, URL https://doi.org/10.1038/srep01627.

[12] T. Lunghi, J. B. Brask, C. C. W. Lim, Q. Lavigne, J. Bowles, A. Martin, H. Zbinden, and N. Brunner, Phys. Rev. Lett. **114**, 150501 (2015), URL https://link.aps.org/doi/10.1103/PhysRevLett.114.150501.

[13] X. Chen, K. Redeker, R. Garthoff, W. Rosenfeld, J. Wrachtrup, and I. Gerhardt, Phys. Rev. A **103**, 042211 (2021), URL https://link.aps.org/doi/10.1103/PhysRevA.103.042211.

[14] L. Childress, M. V. G. Dutt, J. M. Taylor, A. S. Zibrov, F. Jelezko, J. Wrachtrup, P. R. Hemmer, and M. D. Lukin, Science **314**, 281 (2006), URL https://www.science.org/doi/abs/10.1126/science.1131871.

[15] P. Neumann, N. Mizuochi, F. Rempp, P. Hemmer, H. Watanabe, S. Yamasaki, V. Jacques, T. Gaebel, F. Jelezko, and J. Wrachtrup, Science **320**, 1326 (2008), https://www.science.org/doi/pdf/10.1126/science.1157233, URL https://www.science.org/doi/abs/10.1126/science.1157233.

[16] S. Pezzagna and J. Meijer, Applied Physics Reviews **8**, 011308 (2021), https://doi.org/10.1063/5.0007444, URL https://doi.org/10.1063/5.0007444.

[17] G. Waldherr, Y. Wang, S. Zaiser, M. Jamali, T. Schulte-Herbrüggen, H. Abe, T. Ohshima, J. Isoya, J. F. Du, P. Neumann, et al., Nature **506**, 204 (2014), ISSN 1476-4687, URL https://doi.org/10.1038/nature12919.

[18] V. Vorobyov, S. Zaiser, N. Abt, J. Meinel, D. Dasari, P. Neumann, and J. Wrachtrup, npj Quantum Information **7**, 124 (2021), ISSN 2056-6387, URL https://doi.org/10.1038/s41534-021-00463-6.

[19] J. Bowles, M. T. Quintino, and N. Brunner, Phys. Rev. Lett. **112**, 140407 (2014), URL https://link.aps.org/doi/10.1103/PhysRevLett.112.140407.

[20] M. Jerger, Y. Reshitnyk, M. Oppliger, A. Potocnik, M. Mondal, A. Wallraff, K. Goodenough, S. Wehner, K. Juliusson, N. K. Langford, et al., Nature Communications **7**, 12930 (2016), ISSN 2041-1723, URL https://doi.org/10.1038/ncomms12930.

[21] One raw event is formed by one raw bit with its corresponding prepared state and measurement basis.

[22] L. Childress, M. V. G. Dutt, J. M. Taylor, A. S. Zibrov, F. Jelezko, J. Wrachtrup, P. R. Hemmer, and M. D. Lukin, Science **314**, 281 (2006), https://www.science.org/doi/pdf/10.1126/science.1131871, URL https://www.science.org/doi/abs/10.1126/science.1131871.

[23] G. D. Fuchs, V. V. Dobrovitski, D. M. Toyli, F. J. Heremans, and D. D. Awschalom, Science **326**, 1520 (2009), https://www.science.org/doi/pdf/10.1126/science.1181193, URL https://www.science.org/doi/abs/10.1126/science.1181193.

[24] P. Neumann, J. Beck, M. Steiner, F. Rempp, H. Fedder, P. R. Hemmer, J. Wrachtrup, and F. Jelezko, Science **329**, 542 (2010), https://www.science.org/doi/pdf/10.1126/science.1189075, URL https://www.science.org/doi/abs/10.1126/science.1189075.

[25] A. Batalov, C. Zierl, T. Gaebel, P. Neumann, I.-Y. Chan, G. Balasubramanian, P. R. Hemmer, F. Jelezko, and J. Wrachtrup, Phys. Rev. Lett. **100**, 077401 (2008), URL https://link.aps.org/doi/10.1103/PhysRevLett.100.077401.

[26] We have three data-sets and each data-set was measured in different days, so we determine the thresholds for each data-set separately.

[27] X. Chen, K. Redeker, R. Garthoff, W. Rosenfeld, J. Wrachtrup, and I. Gerhardt, *Certified randomness from a remote-state-preparation dimension witness* (2021), URL https://link.aps.org/doi/10.1103/PhysRevA.103.042211.

[28] We have six states in the state preparation stage, and three different measurement settings. As we choose states and measurements randomly, in total there will be 18 different combinations appear with same probability. In each construction of the W_2, we choose 4 states and 2 measurements, which have 8 different combinations in total. So, in one event, we have $\frac{4}{9}$ fraction of data from one plane.

[29] The inverse tangent function in the equation below is in the range 0 to π, which means $0 \leq \tan^{-1} x \leq \pi$.

[30] M. Tomamichel, C. Schaffner, A. Smith, and R. Renner, IEEE Transactions on Information Theory **57**, 5524 (2011).